International Journal of Nanomedicine

Dovepress
open access to scientific and medical research

Open Access Full Text Article

ORIGINAL RESEARCH

The Cleaning Effect of the Photocatalysis of TiO_2-B@anatase Nanowires on Biological Activity on a Titanium Surface

This article was published in the following Dove Press journal:
International Journal of Nanomedicine

Yan Gao[1]
Xi Lin[1]
Yadong Zhao[2]
Shulan Xu[1]
Chunhua Lai[1]
Zehong Guo[1]
Wangxi Wu[1]
Xianglong Ding[1]
Fang Jia[1]
Lei Zhou[1]
Ying Liu[3]

[1]Center of Oral Implantology, Stomatological Hospital, Southern Medical University, Guangzhou 510280, People's Republic of China; [2]Department of Oral and Maxillofacial Surgery, Inner Mongolia People' Hospital, Huhhot, Inner Mongolia 010017, People's Republic of China; [3]Department of Endodontics, Stomatological Hospital, Southern Medical University, Guangzhou 510280, People's Republic of China

Background: Improvements in the early osseointegration of titanium implants require investigations on the bone-implant interface, which is a critical and complex challenge. The surface cleanliness of titanium implants plays an important role at this interface. However, the implant surface would inevitably absorb contamination such as organic hydrocarbons, which is not conductive to the establishment of early osseointegration. Herein, an optimized approach for removing contamination from titanium surfaces was studied.

Methods: The TiO_2-B@anatase NWs (nanowires) were prepared on titanium substrates through a hydrothermal process. A methylene blue degradation experiment was performed to assess the photodegradation activity. The cleaning effect of the photocatalysis of TiO_2-B@anatase NWs on a titanium surface and the cellular early response was determined by analyzing cell morphology, attachment, proliferation and differentiation.

Results: The results indicated that the photocatalysis of TiO_2-B@anatase NWs could effectively remove hydrocarbons on titanium surfaces without sacrificing the favourable titanium surface morphology. The methylene blue degradation experiment revealed that the photocatalysis of TiO_2-B@anatase NWs had powerful degradation activity, which is attributed to the presence of strong oxidants such as $^{\cdot}OH$. In addition, compared to the merely ultraviolet-treated titanium surfaces, the titanium surfaces treated after the NWs photocatalytic cleaning process markedly enhanced cellular early response.

Conclusion: The photocatalysis of TiO_2-B@anatase NWs for the removal of contamination from titanium surfaces has the potential to enable the rapid and complete establishment of early osseointegration.

Keywords: photocatalysis, nanowires, TiO_2, titanium implant, osseointegration

Introduction

Titanium has been widely used for dental implants and orthopaedic surgery due to its excellent physiochemical properties and biocompatibility. The clinical long-term success of implants is related to their early osseointegration. Osteoconduction is defined as appositional bone growth permitting bone formation into the structure of an implant.[1,2] Improvement in the osteoconductive capacity of an implant is the critical factor in improving early osseointegration, requiring focused research efforts on the bone-implant interface.[3,4] Therefore, the surface characteristics of implants play important roles in the progression of osseointegration.[1,5] Most of the challenges of osseointegration focus on improving the surface topography of

Correspondence: Ying Liu
Department of Endodontics, Stomatological Hospital, Southern Medical University, 366 South Jiang Nan Road, Hai Zhu District, Guangzhou 510280, People's Republic of China
Tel +86-20-84408890
Fax +86-20-84433177
Email 286668937@smu.edu.cn

submit your manuscript | www.dovepress.com
DovePress
http://doi.org/10.2147/IJN.S275373

implants to enhance early osseointegration. In addition, the surface energy, chemical composition and time-related bioactivity of titanium merit special attention.[1,6,7] Moreover, surface cleanliness has a significant effect on determining the biocompatibility of implants.[8] The contaminated implant surface has been reported to exhibit disadvantages in osteoconduction that negatively influence the migration and attachment of osteogenic cells[9,10] and even result in failure of the implant.[11] Many studies have reported that the titanium surface adsorbs inorganic ions and organic hydrocarbons or carbon/oxygen-containing species from air in 1 min or even in a few seconds.[12,13] These types of contamination were reported to change the surface chemical composition and the surface energy of implants.[14–16] However, in the product information of clinical dental implants, there is no information for users to know when the products were manufactured, except for the expiration date of the sterilization. This information is useful because a contaminated titanium surface would be unsuitable for early osseointegration.

The generation of a superhydrophilic titanium surface by ultraviolet (UV) irradiation was discovered in 1997.[17] This unique change of the titanium surface provides advantages for the cellular responses to an implant, including cell attachment, proliferation and differentiation.[6,10,18] These excellent properties are ascribed to the changed surface chemical composition due to the photocatalytic activity of TiO_2. Two possible mechanisms could account for these properties, including the conversion of the relevant Ti^{4+} sites to Ti^{3+} sites, which are favourable for dissociative water adsorption and the removal of hydrocarbons.[7,18,19] However, most titanium surfaces were UV-treated in air in previous studies;[6,7,18,19] therefore, the titanium surface is inevitably exposed to the air during or after UV irradiation, which could cause further problems with contamination, as exposure to air is also not suitable for clinical applications. Furthermore, the crystal phase and photocatalyst concentration are two important impact factors of the photocatalytic activity of TiO_2.[20,21] A previous study confirmed that there is an absence of the crystal phase of TiO_2 after acid-etched titanium at a high temperature.[19] Consequently, the altered surface chemical composition and the hydrophilic phase are attributed to the photocatalysis of TiO_2 that forms a thin oxide film on the titanium surface in the air. The thickness of the TiO_2 oxide film plays an important role in photocatalysis.[22] Moreover, enhanced photocatalysis can be achieved by sputtering TiO_2 particles onto the titanium surface.[23] These observations indicate that the photocatalytic activity generated by only a small amount of TiO_2 oxide film oxidized in the air may not sufficiently remove contamination on the titanium surface.

Recently, one-dimensional nanostructures, such as anatase phase TiO_2 nanowires, have provided greater photocatalytic degradation of organic pollutants because their photogenerated charge carriers recombine at the lowest rate in anatase[24–26] with a larger surface area[20] and efficient charge transfer.[27] However, the recombination of photogenerated electrons and holes in anatase is still rapid, which limits the photocatalytic activity of anatase.[28] TiO_2-B is a metastable monoclinic modification of TiO_2, and its energy bandgap is very close to that of anatase.[29] Therefore, the energy bandgap similarity and electronic energy level differences can boost the charge transfer from one phase to the other if anatase and TiO_2-B are combined together, resulting in enhanced photocatalytic activity. Recently, TiO_2-B@anatase nanowires have been successfully prepared and were found to exhibit excellent photocatalytic degradation activity.[28]

In fact, photocatalysts such as TiO_2 have been widely used in the field of water pollution control. In this article, we propose that the preparation of a photocatalyst with strong photocatalytic activity for TiO_2-B@anatase nanowires can effectively remove contamination on the titanium surface by photocatalysis. The objectives of this study were to provide a new approach for removing contamination from titanium surfaces, which would be beneficial for establishing early osseointergration, and to examine the cleaning effect of the photocatalysis of TiO_2-B@anatase nanowires on a titanium surface. In addition, the early cellular behaviours and functions of cells in vitro and potential bone-titanium integration in vivo on photocatalytically cleaned titanium surfaces were explored.

Methods

Synthesis of TiO_2-B@ Anatase Core-Shell NWs

TiO_2-B@anatase NWs were prepared according to a previously described method.[28] Briefly, titanium disks (15 millimetres (mm) in diameter, 1.5 mm in thickness) surfaces were ground with 400 grit, 600 grit, 800 grit and 1000 grit SiC papers and ultrasonically cleaned with acetone, absolute ethanol and distilled water for 15 minutes (min) twice in series. Next, the titanium disks were placed at an angle against the walls of a 25 millilitre (mL)

Teflon-lined stainless-steel autoclave filled with 10 mL of 1 mole per litre (M) aqueous NaOH solution. The autoclave was kept inside an oven at 220°C for 8 hours (h). After the autoclave was cooled, the titanium disks covered with sodium titanate NWs were removed from the Teflon-lined vessel and washed with ultrapure water before immersion in 0.02 M hydrochloric acid for 1 h to exchange Na^+ with H^+. The sodium titanate NWs were then transformed to hydrogen titanate NWs. Next, the hydrogen titanate NWs were placed in 200 mL of titanium tetrachloride ($TiCl_4$) solution and kept at 50°C for 4 h to develop anatate nanocrystals around the hydrogen titanate NWs. The $TiCl_4$ solution was prepared by mixing 0.18 mL of $TiCl_4$ with 0.8 mL of hydrochloric acid (HCl) solution (36–38% by weight), with deionized water added to reach a final volume of 200 mL. Finally, the hydrogen titanate NWs covered with anatate nanocrystals were calcined at 500°C for 1 h to convert the hydrogen titanate NWs to TiO_2-B@anatase NWs.

Characterization of the NWs

The morphology of the TiO_2-B@anatase NWs was observed using field emission scanning electron microscopy (FESEM, JSM-6330F, JEOL, Japan) and high-resolution transmission electron microscopy (HRTEM, JEM-2010, JEOL, Japan). The crystalline structure of the nanowires was determined using X-ray diffraction (XRD, D8 ADVANCE, Bruker, Germany) with a Cu Kα radiation source (λ=0.15418 nm, 40 kV, 40 mA) and scanning the diffraction angle from 20 to 60 degrees at a scanning speed of 0.2 degrees per second.

Photocatalytic Activity

A schematic diagram of the experimental setup is shown in Figure 1. The photoreactor consisted of one 15-Watt (W) bactericidal UV-C lamp (Philips, Amsterdam, Holland) (λ=250±20 nm) with a quartz tube placed in the centre of the cylindrical container with a capacity of 300 mL. The TiO_2-B@anatase NWs solution was circulated through the reactor system using a peristaltic pump (Langyin, Guangzhou, China) at a flow rate of 1000 revolutions per minute (rpm), with the reactor operating in recirculation mode.

The generation of ·OH radicals under UV light irradiation was analysed via the fluorescence technique using terephthalic acid, which readily reacted with ·OH radicals to generate a fluorescent product, 2-hydroxyterephthalic acid.[24,30] One hundred milligrams (mg) of the prepared TiO_2-B@anatase nanowires that were ultrasonically detached from the titanium disks were added to 500 mL of 5×10^{-4} M terephthalic acid in a 2×10^{-3} M NaOH solution. The mixture was ultrasonicated for 15 min to disperse the nanowires and then added to the photoreactor. The mixture was circulated in a dark room at room temperature for 1 h to reach adsorption equilibrium and was later irradiated using a UV lamp for 2 h. The sample solution was extracted every 15 min and filtered through a 0.22-micrometer (μm) membrane filter, followed by analysis using a fluorescence spectrophotometer (SpectraMax M5, Molecular Devices, USA) at a wavelength of 425 nm, which corresponded to the fluorescence peak intensity of the product of 2-hydroxyterephthalic acid.

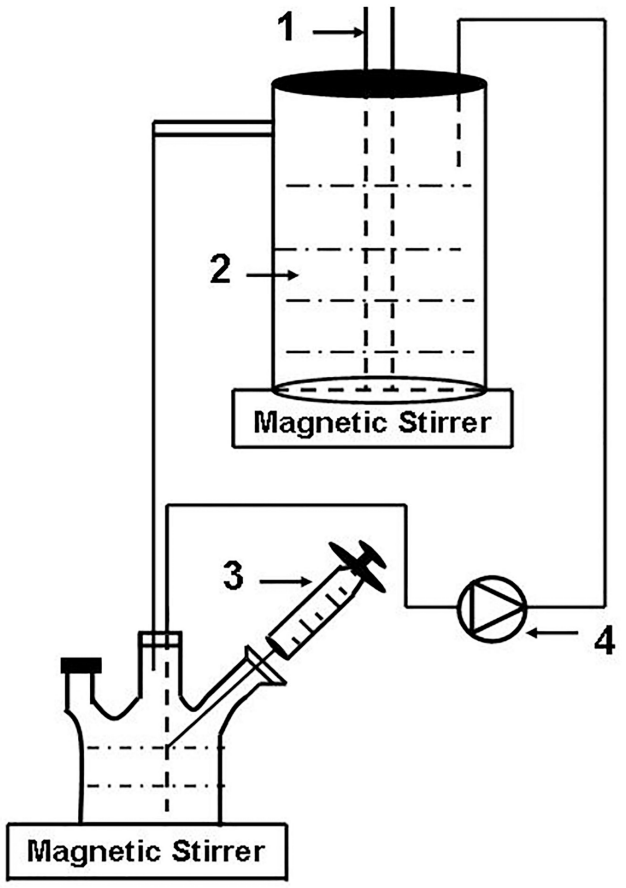

Figure 1 Schematic diagram of the experimental setup. 1 UV lamp. 2 TiO_2-B@anatase nanowires aqueous solution. 3 Sampling. 4 Peristaltic pump.

To assess the photodegradation activity, 100 mg of the prepared TiO_2-B@anatase NWs and TiO_2 nanoparticles (NPs) were added to 500 mL of methylene blue (MB) aqueous solution ($C_{methylene\ blue}$=10 ppm). As previously stated, the mixture solution was circulated in a dark room at room temperature for 1 h and later irradiated using a UV lamp for 2 h. The sample solution was extracted every 15 min and filtered through a 0.22 μm membrane filter,

followed by analysis using a spectrophotometer (SpectraMax M5, Molecular Devices, USA) at a wavelength of 664 nm, which corresponded to the peak optical density of methylene blue.

Titanium Disks Cleaning and Surface Characterization

The SLA (sandblasting with large grit and acid-etching) titanium disks (15 mm in diameter, 1 mm in thickness) were sandblasted using Al_2O_3 particles and etched using a mixture of 18% HCl and 49% H_2SO_4 at 60°C for 30 min and then ultrasonically cleaned twice in deionized water for 15 min. The prepared surfaces were used for the experiments after storage in sealed containers under dark ambient conditions for 4 weeks. The SLA disks were hung in the photoreactor, and the surfaces prepared for cleaning faced the light. Next, 500 mL of the TiO_2-B@anatase NWs aqueous solution was circulated in a dark room at room temperature for 1 h and later irradiated with a UV lamp for 2 h. Finally, the SLA disks were ultrasonically cleaned twice in deionized water for 15 min to remove the nanowires attached onto the titanium surface. The titanium disks were divided into four groups: SLA, NWs-SLA, UV-SLA and NWs+UV-SLA. The NWs-SLA and NWs+UV-SLA groups were treated as mentioned above, while the NWs-SLA group was treated without UV irradiation in water. The SLA group was the control group. The UV-SLA group was treated with UV irradiation in water. All specimens were then stored in deionized water and sterilized via irradiation with a dose of 25 kGy for 12 h.

The surface morphology of the titanium disks was characterized via SEM. XRD experiments identified the crystalline phase of the surfaces of the titanium disks. The three-dimensional profile of the surfaces of the titanium disks was measured using an optical profilometer (Breitmeier Messtechnik GmbH, BMT, Germany), and the surface roughness parameter Ra was measured over a scanning area of 300 μm × 300 μm. The hydrophilicity of the titanium surface was determined by measuring the contact angle of 1 μL of H_2O using a contact angle measuring device (OCA40, Dataphysics, Germany). The elements and chemical composition of the titanium surface were evaluated via X-ray photoelectron spectroscopy (XPS) (ESCALAB 250, Thermo Fisher Scientific, US) under high vacuum conditions. This XPS system was equipped with a monochromatic Al Kα X-ray source (hv=1486.6 ev photons) at a 90° take-off angle. The binding energy was calibrated by the C 1s (C-C, C-H) contribution at 284.8 eV.

Osteoblastic Cell Experiment

Human osteoblast-like MG-63 cells (the Laboratory of cell biology of Southern Medical University, Guangzhou, China), isolated from human osteosarcoma, were placed into Dulbecco's modified Eagle's medium (DMEM; HyClone, Thermo Fisher Scientific, US) supplemented with 10% fetal bovine serum and 1% antibiotic solution (penicillin-streptomycin; HyClone). The cells were cultured at 37°C under a humidified atmosphere of 5% CO_2. The cells were detached using 0.25% trypsin-EDTA-4Na (HyClone) when they reached 80% confluency and seeded onto the titanium disks that were placed in 24-well plates at a density of 1×10^4 cells/cm^{2}cells/cm^2. The culture medium was renewed every two days. Based on the above experimental results, without UV irradiation, only the NWs treatment had no effect on the titanium surface. The titanium disks were divided into three groups in the cell experiment: SLA, UV-SLA and NWs+UV-SLA.

The migration of MG-63 cells to the titanium surface was evaluated using a dual-chamber transwell migration assay. The cells were detached from the culture plates using trypsin and then washed twice in DMEM and resuspended at a density of 1.5×10^5/mL in DMEM. Two hundred microlitres of the cell suspension was seeded into the upper chamber of a polyester membrane with an 8-μm pore size. The titanium disk was placed at the bottom of the lower chamber, and 500 μL of DMEM culture solution containing 10% foetal bovine serum was added. After 12 h of incubation, the cells were fixed with 4% paraformaldehyde for 30 min and then stained with 0.1% crystal violet. The nonmigratory cells on the upper surface of the membrane were removed, and the migrated cells were counted in six random fields at a magnification of 400×.

The initial attachment of the cells was measured by calculating the fluorescently stained nuclei on the titanium surface after 1 h, 2 h and 4 h of incubation. At each selected time point, the non-adherent cells were removed from the titanium surface after rinsing with phosphate buffered saline (PBS, HyClone). The adherent cells on the titanium were fixed with 4% paraformaldehyde for 30 min. Some of the samples were sputter-coated with Au/Pd for observation using SEM (JSM-6330F, JEOL, Japan) at a magnification of 2000×. The remaining samples were then stained with the fluorescent dye rhodamine

phalloidin (Alexa Fluor 635, Invitrogen, USA) for 30 min in dark ambient conditions. The number of adherent cells was estimated by counting the number of red stained actin filaments using a fluorescence microscope (IX51, Olympus, Japan) (magnification, 100×; area, 1800 × 1350 μm^2). Four different fields of each disc were selected randomly to evaluate cell attachment.

After 8 h of culturing, the titanium surfaces were rinsed three times using PBS, and then the cells were fixed in 4% paraformaldehyde for 30 min. Next, the fixed cells were permeabilized using 0.1% Triton X-100 in PBS for 5 min and then blocked with 1% bovine serum albumin (BSA/PBS) for 30 min. Protected from light, the cells were then stained with Hoechst 33,342 (nuclei blue colour) and rhodamine phalloidin (actin filament red colour). Confocal laser scanning microscopy was used to observe the cell morphology and cytoskeletal arrangement (magnification, 600×).

Cell proliferation was evaluated using a tetrazolium salt (MTS)-based CellTiter 96® AQ_{ueous} proliferation assay at culture days 1, 3 and 5. At each prescribed time, the titanium disks were gently rinsed using PBS and transferred into a new 24-well plate. Then, 500 μL of DMEM was added to each well, followed by 100 μL of MTS reagent. After the mixture was incubated at 37°C for 3 h, 100 μL of the culture solution was transferred to a 96-well plate for measurement using a microplate reader (SpectraMax M5, Molecular Devices, USA) at 490 nm.

The ALP activity of osteoblasts was examined by colourimetry-based assays using the ALP reagent SIGMAFAST p-Nitrophenyl phosphate Tablets (*p*-NPP) (Sigma-Aldrich, Missouri, USA). After 3 d, 7 d and 14 d of incubation, the cells were washed three times using PBS and incubated in 200 μL 1% Triton X-100 for 40 min at 37°C. 50 μL solution was transferred into a 96-well plate and incubated with 200 μL of *p*-NPP reagent solution at 37°C for 30 min. The ALP activity was evaluated by the amount of nitrophenol released and measured at 405 nm using a microplate reader (SpectraMax M5, Molecular Devices, USA).

ALP gene expression was quantitatively analysed using fluorescence real-time quantitative PCR (FQ-PCR) after cell culture for 7 and 21 d. Total mRNA was obtained using TRIzol (Takara Bio, Kyoto, Japan) and purification. Reverse transcription was performed using the PrimeScriptR RT reagent kit (Takara Bio, Kyoto, Japan). The complementary DNA was generated using the SYBR Premix DimerEraser kit (Takara Bio, Kyoto, Japan). ALP primer designs and PCR conditions were established previously.[26] The GAPDH gene was amplified as a normalized control.

The mineralization capability of cells on the titanium surface was examined by alizarin red staining. After 14 days of incubation, specimens were washed twice with PBS and then fixed with 4% paraformaldehyde for 30 min. The titanium disks were rinsed and stained with 40 mM alizarin for 20 min. Subsequently, the disks were washed with ddH_2O. After drying in air, mineralized nodules on titanium surfaces emerged.

Statistical Analyses

There were six samples for the cell studies, except for the cell attachment assay, which was examined for 4 different fields in 3 samples of different groups. One-way ANOVA was used to analyse the effects of UV photocatalysis cleaning. A post-hoc Bonferroni test was used to assess differences between the control and the test groups, if necessary. All statistical analyses were performed using SPSS 26.0 software (© 2004 by SPSS Inc.), where $p<0.05$ was considered to be statistically significant and $p<0.01$ was considered to be highly statistically significant.

Results

Structural and Chemical Characterizations of the NWs

A schematic diagram of the formation process of TiO_2-B@anatase NWs is shown in Figure 2.

FESEM and TEM images of sodium titanate NWs and TiO_2-B@anatase NWs are shown in Figure 3A–H. Sodium titanate NWs were generated on the titanium disk surface after alkali-heat treatment at 220°C for 8 h. The nanowires were abundant in quantity and quite clean with smooth surfaces (Figure 3A, C and E). After immersion in a $TiCl_4$ solution for 3 h to form anatase nanocrystals followed by calcination at 500°C for 1 h, the sodium titanate NWs were transformed into TiO_2-B@anatase NWs, which were covered with spines and apparently round and rough (Figure 3B and D). Figure 3F further illustrates that the hierarchical anatase nanocrystal arrays formed a thick layer over the surface of sodium titanate NWs. Figure 3G is a typical HRTEM image of a core-shell NWs. The average diameter of the sodium titanate NWs was approximately 100 nm, which was thinner than the TiO_2-B@anatase NWs diameter (~130 nm). Figure 3H displays an HRTEM image captured

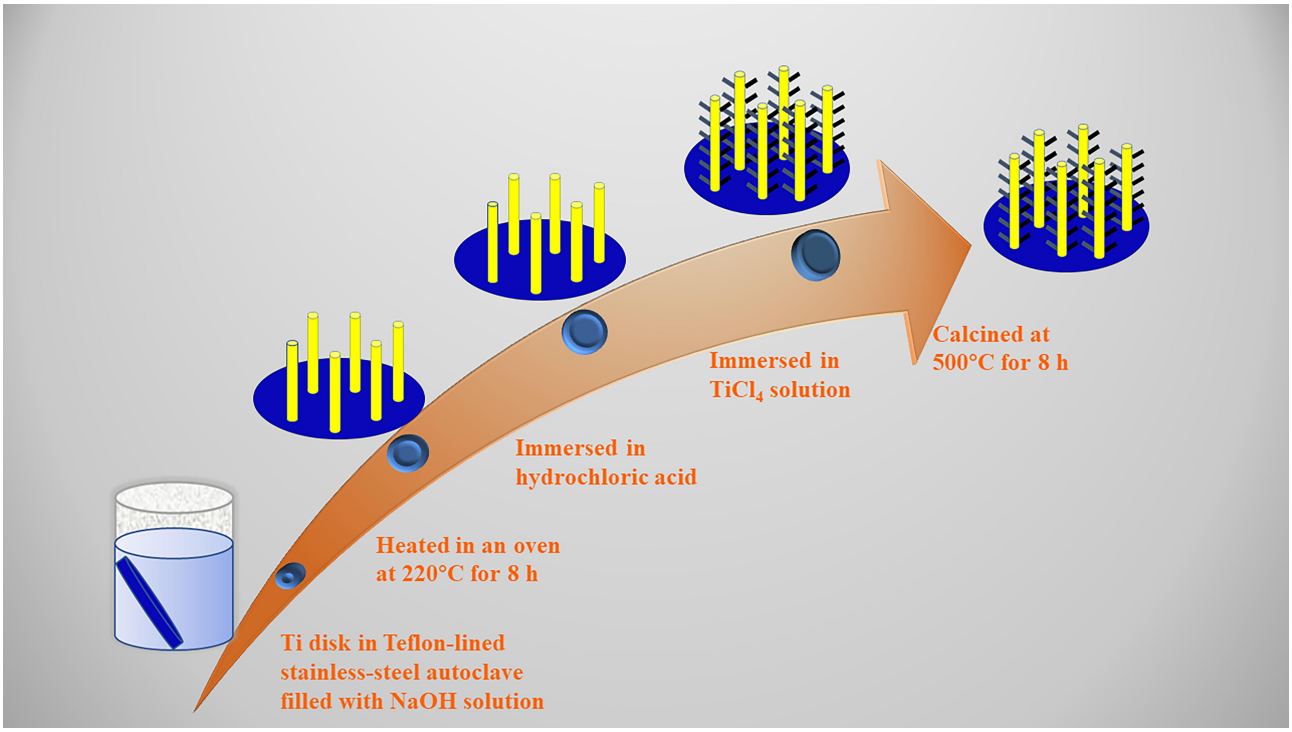

Figure 2 Schematic route diagram of the formation process of TiO_2-B@anatase nanowires. In the first step, sodium titanate nanowires were self-assembled hydrothermally onto the titanium substrate surface. Next, the sodium ions were exchanged with protons to convert the sodium titanate nanowires to hydrogen titanate nanowires. Finally, TiO_2-B@anatase nanowires were fabricated by immersing hydrogen titanate nanowires in $TiCl_4$ solution to form anatase phase nanowires, followed by calcination at 500°C.

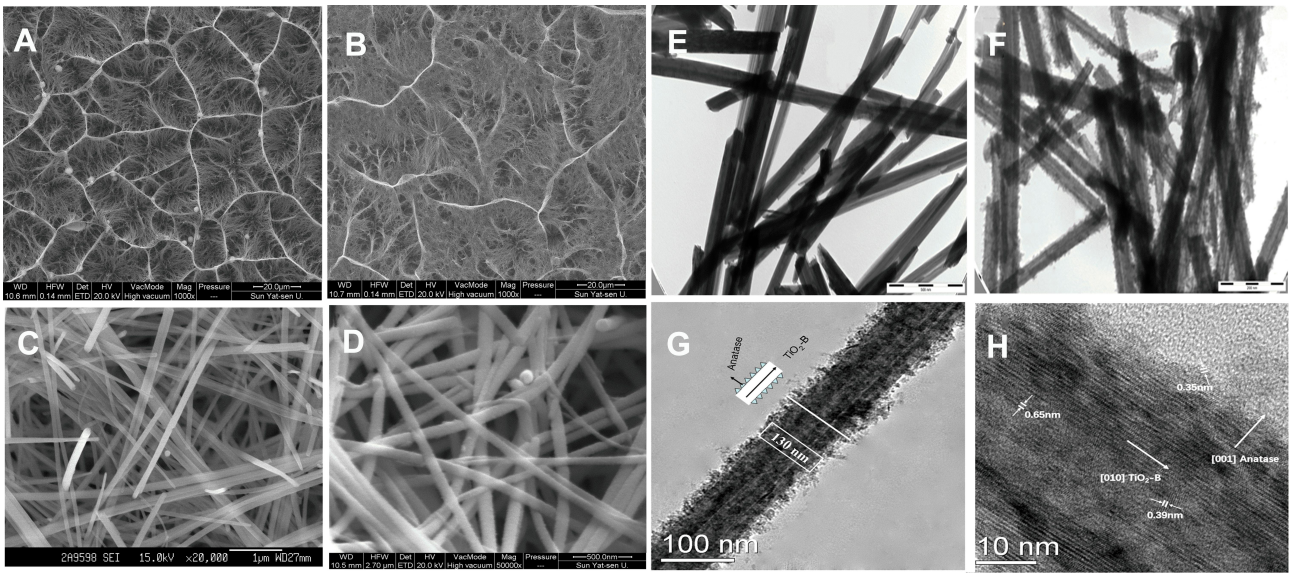

Figure 3 (**A, C** and **E**) FESEM and TEM images of the hydrogen titanate nanowires. (**B, D** and **F**) FESEM and TEM images of TiO_2-B@anatase nanowires (Bar = 500 nm). (**G** and **H**) Typical HRTEM image of a TiO_2-B@anatase core-shell nanowire.

near the interface between the TiO_2-B core and anatase nanocrystal shell NWs. The lattice spacing between adjacent lattice planes of the TiO_2-B core was approximately 0.65 nm and 0.39 nm, while the anatase nanocrystal shell was clearly visible at 0.35 nm. The HRTEM images confirmed that single-crystal anatase grew on the TiO_2-B core NWs. The TiO_2-B core and anatase shell crystal structures were well matched. This kind of transition from one crystalline phase to the other could facilitate interfacial charge transfer to enhance photocatalysis.

The diffraction peaks of the NWs after each step of the synthesis are shown in Figure 4. The Ti (JCPDS#44-1294) diffraction peaks in Figure 4A are attributed to the titanium substrate. After the high temperature and pressure reaction, the diffraction of sodium titanate NWs could be detected on the titanium surface (Figure 4B). In Figure 4C, the diffraction pattern is consistent with the body-centred orthorhombic $H_2Ti_2O_5{\cdot}H_2O$ phase, which contains two-dimensional sheets of edge sharing TiO_6 octahedra.[28,31] Although the diffraction pattern in Figure 4D is similar to that of Figure 4E, well-resolved anatase diffractions can be distinguished from the $H_2Ti_2O_5{\cdot}H_2O$ phase. This result further confirms that anatase nanocrystals formed on the surface of hydrogen titanate NWs after immersion in $TiCl_4$ solution. Figure 4E shows the diffraction pattern of the NWs after calcination. It was reported that if the calcination temperature is increased above 650°C, then the $H_2Ti_2O_5{\cdot}H_2O$ phase can be transformed into anatase.[28] Therefore, after calcination at 500°C in the present study, the diffraction peak widening can be attributed to the coexistence of TiO_2-B and anatase.

Photocatalytic Activity of the NWs

The fluorescence emission spectrum of the terephthalic acid solution was measured every 15 min during irradiation at an excitation wavelength of 315 nm. As shown in Figure 5A (Supplementary Table S1), the spectrum had an identical shape and maximum emission wavelength to that of 2-hydroxyterephthalic acid, which indicated that ·OH was generated during TiO_2-B@anatase NWs photocatalysis. It shows the alteration of the fluorescence intensity with illumination time at 425 nm. Almost no ·OH radicals were generated without UV treatment or without the NWs photocatalyst. Moreover, the fluorescence intensity increased over time under the action of TiO_2-B@anatase NWs photocatalysis, especially during the first 15 min, and reached a maximum at 75 min (Figure 5B, Supplementary Table S2).

The photocatalytic activity of TiO_2-B@anatase NWs was investigated by the degradation of MB. The remaining concentration of MB in the solution was measured and plotted at each selected time. As shown in Figure 5C (Supplementary Table S3), the peak optical density of MB at approximately 664 nm gradually decreased with increasing illumination time. More importantly, a remarkable decrease in the optical density could be observed during the first 15 min, indicating that the degradation rate of MB is prominent during this time. The photodegradation activity of TiO_2 nanoparticles and TiO_2-B@anatase NWs is reflected in Figure 5E. We may conclude that the relative

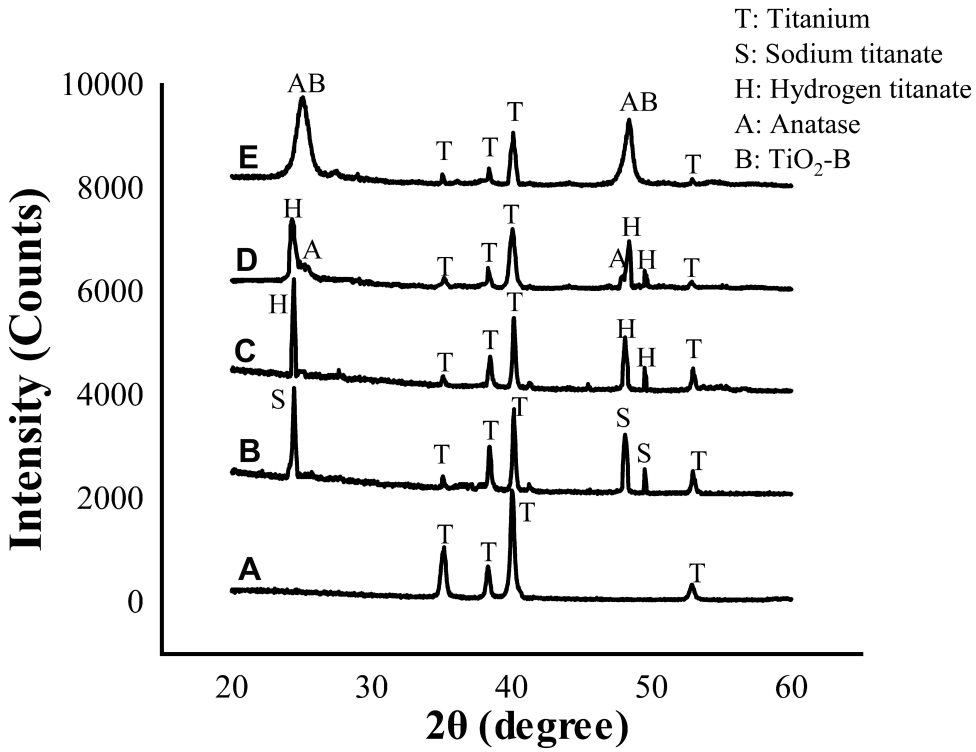

Figure 4 X-ray diffraction patterns of (**A**) titanium disk, (**B**) sodium titanate nanowires, (**C**) hydrogen titanate nanowires, (**D**) hydrogen titanate nanowires decorated with anatase, and (**E**) TiO_2-B@anatase nanowires.

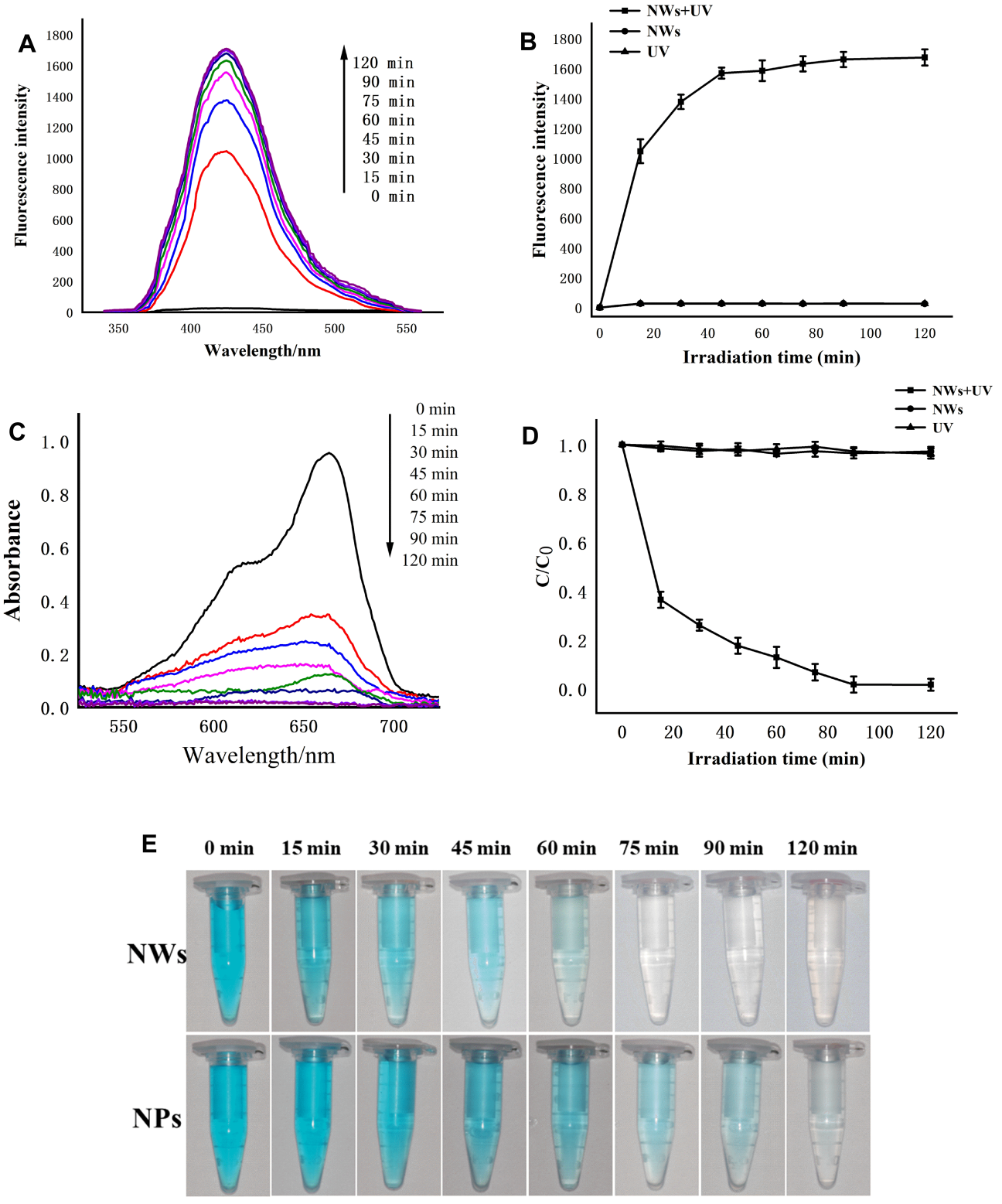

Figure 5 (**A**) Fluorescence spectral changes detected during irradiation of TiO_2-B@anatase nanowires for 2 h in 2×10^{-3} M NaOH solution of terephthalic acid (excitation at 315 nm). (**B**) Fluorescence intensity of the samples in the corresponding time interval. (**C**) The change in the absorbance value of MB under the photocatalytic activity of TiO_2-B@anatase NWs at each selected time. (**D**) The change in the normalized concentration (C/C_0) of MB with irradiation time. (**E**) Comparison of the photodegradation activity of MB between TiO_2 nanoparticles and TiO_2-B@anatase NWs.

photodegradation rate of TiO_2-B@anatase NWs exhibited significant improvement compared to TiO_2 nanoparticles. The colour of the MB faded over time and became transparent at approximately 75 min of illumination in the TiO_2-B@anatase NWs group. The normalized concentration (C/C_0) changes of MB with irradiation time should be proportional to the normalized absorbance (A/A_0). As shown in Figure 5D (Supplementary Table S4), only a slight decrease in the MB concentration was observed in the presence of either UV or nanowire photocatalyst exposure alone, which implies that both the light source and the photocatalyst are necessary for photodegradation to occur.

Surface Characterization of the Titanium Surface After Photocatalytic Cleaning

The SEM images revealed that the SLA, UV-SLA, NWs-SLA and NWs+UV-SLA samples were characterized by similar multilevel pores (Figure 6A and B), including the primary roughness due to 10–30 μm diameter features generated by sandblasting and the secondary roughness with a honeycomb structure in the range of 1–3 μm diameter formed by acid etching. After XRD analyses (Figure 6C), the SLA surface exhibited only diffraction patterns attributed to Ti metal and did not exhibit any other peaks of crystalline structure. As shown in the three-dimensional reconstructed image (Figure 6D), the surface roughness parameter Ra of the SLA was 1.56 ± 0.32 μm, which was similar to that of the other groups.

The measured contact angles are displayed in Figure 7A–D. The contact angle of a H_2O droplet on the SLA surface was 110°, while after exposure to UV light or after the NWs+UV photocatalytic cleaning treatment of the SLA surface for 2 h, both contact angles decreased to 0°. However, for only the NWs photocatalyst treatment, the contact angle did not change very much.

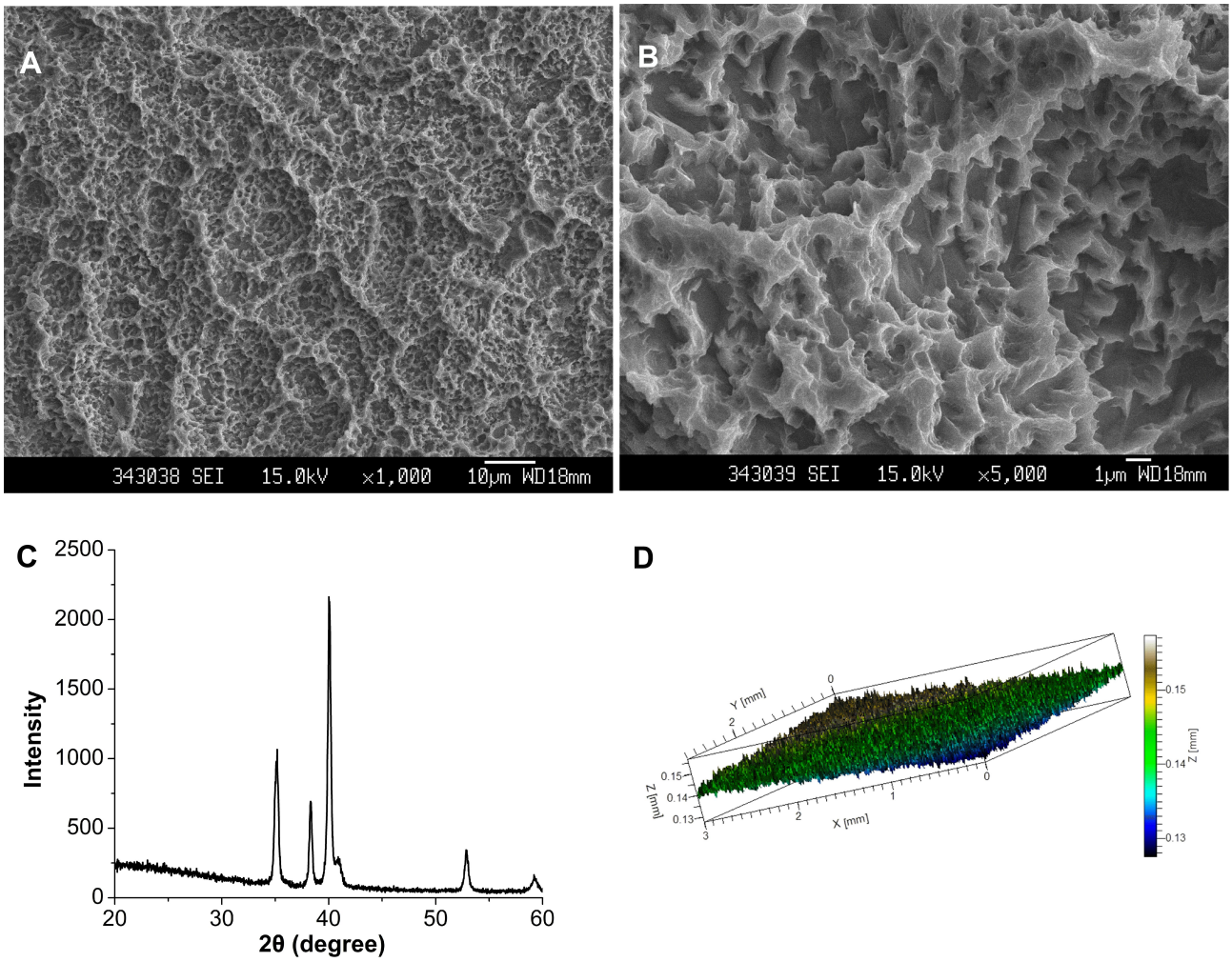

Figure 6 (**A** and **B**) SEM image of an SLA surface used in this study ((**A**) 1000×, (**B**) 5000×). (**C**) X-ray diffraction spectrum of the SLA surface. (**D**) Three-dimensional reconstructed image of an SLA surface.

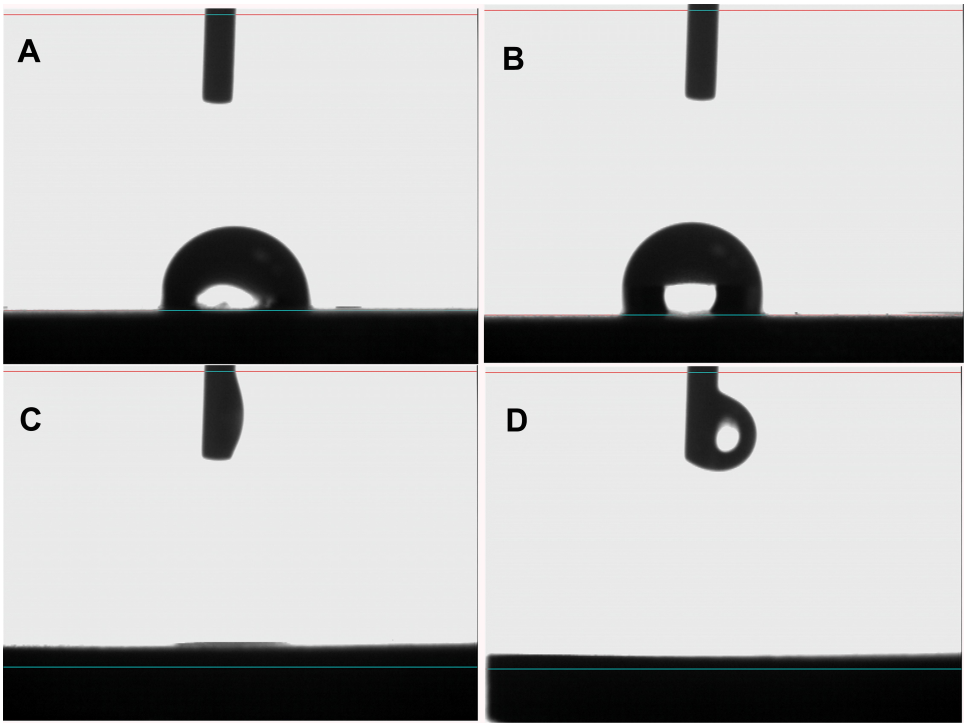

Figure 7 Photographic images of H_2O droplets pipetted onto the titanium surfaces: (**A**) SLA, (**B**) NWs-SLA, (**C**) UV-SLA, and (**D**) NWs+UV-SLA.

The XPS high-resolution spectra of C 1s, O 1s and Ti 2p from the SLA surface of the different groups are shown in Figure 8A–C (Supplementary Tables S5-S7). From the C 1s spectra, the C 1s peak at approximately 284.8 eV that is ascribed to hydrocarbons (C-C, C-H)[10,32,33] decreased after UV or NWs+UV treatment. This is especially true after NWs +UV treatment for 2 h when the content of C decreased from 49.49% to 25.3% but was basically remaining unchanged after the NWs treatment (Figure 8D). Meanwhile, the O 1s peak at approximately 530.1 eV assigned to TiO_2 (O^{2-})[33] and at approximately 531.3 eV fitted to Ti-OH[34,35] increased after the UV or NWs+UV treatments. Compared with the SLA and NWs-SLA groups, the Ti $2p_{3/2}$ peaks at approximately 458.5 eV and Ti $2p_{1/2}$ peaks at approximately 464.2 eV were both slightly shifted to a higher energy for the UV-SLA and NWs+UV-SLA surfaces. In combination with the XPS spectra of O 1s and Ti 2p, these data indicated that the surfaces of the substrates were oxidized to stoichiometric TiO_2 layers,[19] especially on the surfaces of the NWs+UV-SLA group.

Cell Migration, Attachment and Morphology

The effect of photocatalytic cleaning on the migration capacity of MG-63 cells was evaluated via a transwell migration assay. The assay results demonstrated that the SLA surface had a positive affinity for the cells after photocatalytic cleaning. After 12 h incubation, the number of migrated cells to the NWs+UV-SLA surfaces was 2-fold greater than that of the SLA surfaces ($p < 0.01$) and 10% greater than that of the UV treatment alone ($p<0.05$) (Figure 9A–C, Figure 9J, Supplementary Table S8).

The image of the MG-63 cells attached onto the titanium surfaces after 2 h incubation is presented in Figure 9D–F, with the red stained actin filament directly counted on fluorescently stained images at 100×. Figure 9L–T shows the morphology of cells cultured on the different titanium surfaces after 1 h, 2 h, and 4 h of culturing. The cells on the titanium surfaces were all round-shaped after 1 h of incubation. Cells on the UV-SLA and NWs+UV-SLA surfaces turned into an oval shape after 2 h incubation. After 4 h of culture, the cells on the UV-SLA showed slender filopodia, while sturdy lamellipodia were present on the NWs+UV-SLA surfaces. The cell attachment rate on the SLA, UV-SLA and NWs+UV-SLA surfaces gradually increased with the cell attachment rate on the NWs+UV-SLA surfaces exhibiting better performance than those of the other two surfaces ($p<0.01$) (Figure 9K, Supplementary Table S9).

Figure 9G–I show the immunofluorescent images of MG-63 cells on different surfaces after 8 h incubation. Red-stained

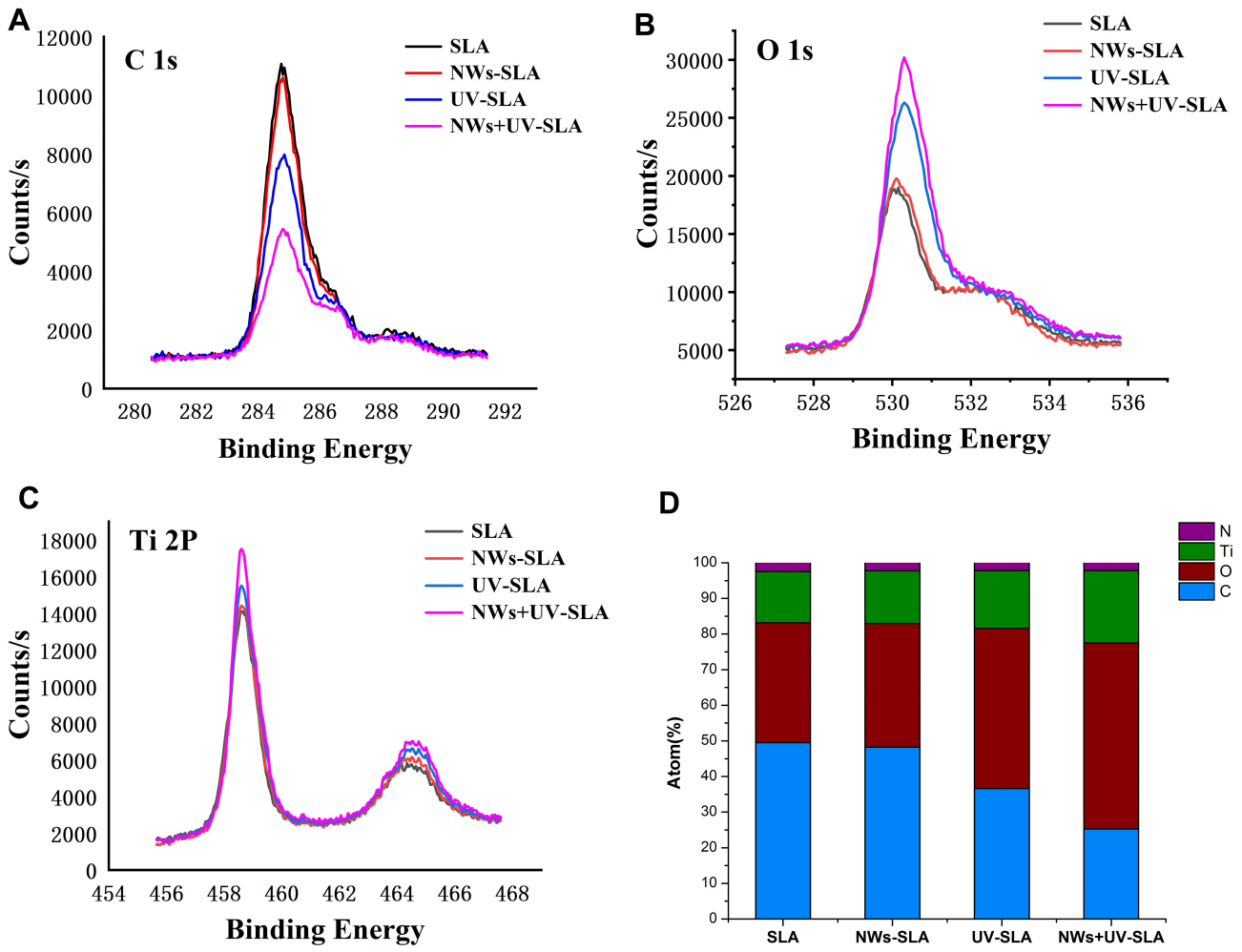

Figure 8 (**A**–**C**) Changes in the XPS profile for C 1s, O 1s and Ti 2p. (**D**) Atomic percentages of the SLA, NWs-SLA, UV-SLA and NWs+UV-SLA surfaces.

actin was the main cytoskeleton arranged around the blue nuclei. Most of the cells had begun to spread and displayed a morphology similar to that of a triangle or polygon. Furthermore, the cells on the UV-SLA and NWs+UV-SLA surfaces extended further; in particular, some of the spindle-like filopodia exhibited a more extensive arrangement on the NWs+UV-SLA surfaces.

Cell Proliferation and ALP Activity

The cell proliferation evaluated via an MTS assay is shown in Figure 10A (Supplementary Table S10). Cell proliferation increased over time on three different surfaces after 1 d, 3 d and 5 d of culture. The NWs+UV-SLA surface exhibited greater proliferative activity than the other two surfaces, especially at 3 d and 5 d of incubation ($p<0.01$). Compared to the SLA surface, the UV-SLA surface exhibited superior performance at 3 d ($p<0.05$) and improved at 5 d after seeding ($p<0.01$).

The ALP activity was determined to evaluate the early differentiation of MG-63 cells. As presented in Figure 10B (Supplementary Table S11), there was no significant difference in the differentiation activity of the cells among the groups at 3 d of incubation ($p>0.05$). The ALP activities of the cells on the three groups of surfaces increased at 7 d after the seeding was performed, with the NWs+UV-SLA surface exhibiting a greater ALP activity than those of the other two surfaces. However, the ALP activity of the cells decreased at 14 d of incubation among the three groups, but the ALP activity on the NWs+UV-SLA surface was still higher than that of the SLA surface ($p<0.05$). Consistent with the results above, as presented in Figure 10C (Supplementary Table S12), the expression of ALP on the NWs+UV-SLA surface was greater than those of the other groups at 7 days. On day 14 of culture, the area of mineralized nodules detected by alizarin red staining was also greater on the NWs+UV-SLA surface (Figure 10D).

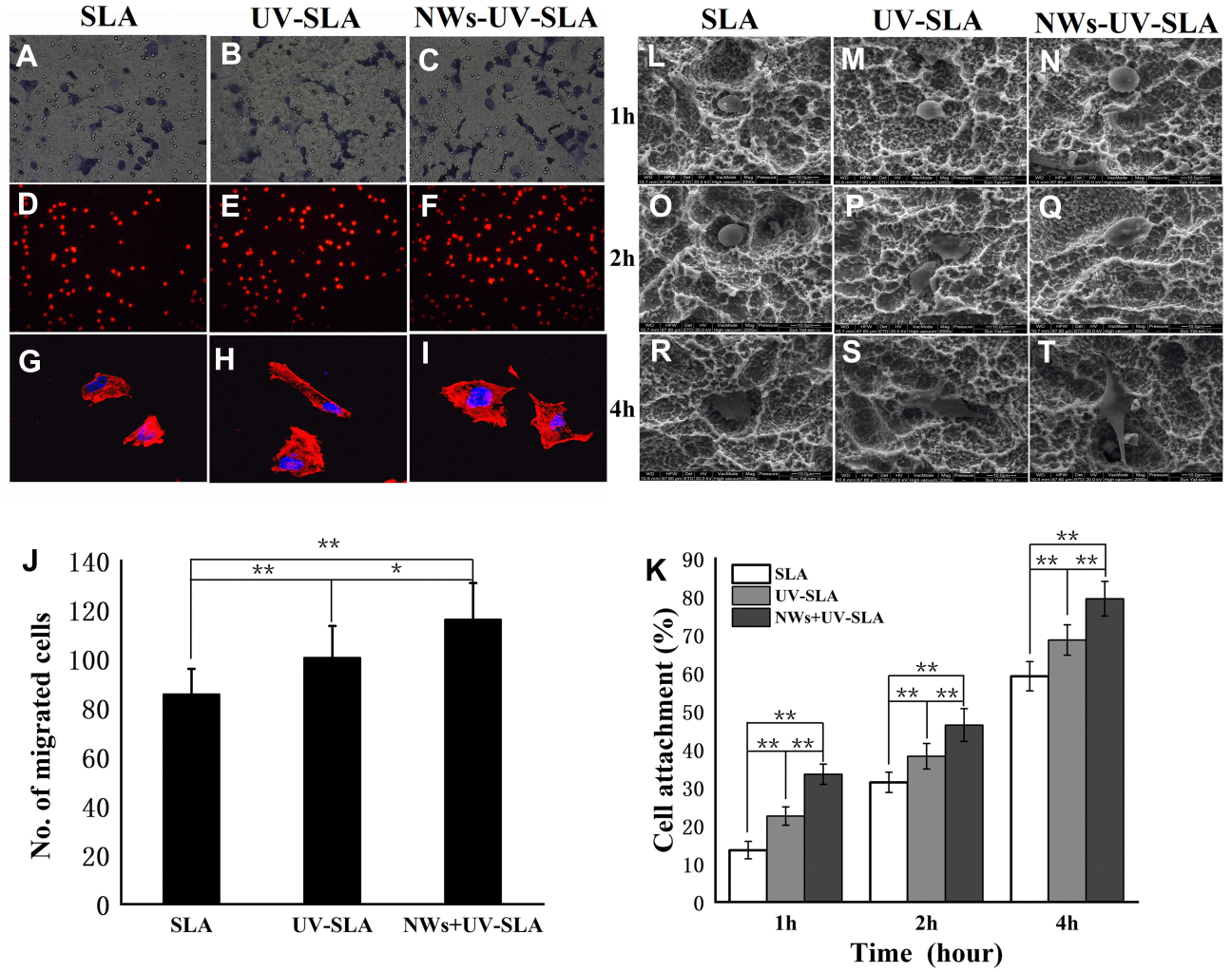

Figure 9 (**A**–**C**) Osteoblast-attracting ability of three differently conditioned titanium surfaces at 12 h of incubation (Bar=50 μm). (**D**–**F**) Images of the fluorescently stained actins of MG-63 cells attached on different surfaces after 2 h of incubation (Bar=100 μm). (**G**–**I**) Initial cellular spread and cytoskeletal arrangement on titanium surfaces. Confocal microscopic images of MG-63 cells after 8 h incubation. (**J**) The number of cells migrating to titanium surfaces after 24 h of incubation. (**K**) The adhesion rate of cells on the titanium surfaces after 2 h of incubation. (mean±SD, n=6; *p<0.05, **p<0.01). (**L**–**T**) SEM images of the morphology of cells cultured on the different titanium surfaces after 1 h, 2 h, and 4 h of culture (2000×, bar=10).

Discussion

In this study, TiO_2-B@anatase NWs were prepared on titanium substrates through a four-step process. In the first step, sodium titanate NWs were self-assembled hydrothermally onto the titanium substrate surface. Next, the sodium ions were exchanged with protons to convert the sodium titanate NWs to hydrogen titanate NWs. Finally, TiO_2-B@anatase NWs were fabricated by immersing hydrogen titanate NWs in $TiCl_4$ solution to form anatase phase NWs, followed by calcination at 500°C.

The HRTEM images confirmed that single-crystal anatase grew on the TiO_2-B core NWs. The TiO_2-B core and anatase shell crystal structures were well matched. This kind of transition from one crystalline phase to the other could facilitate interfacial charge transfer to enhance photocatalysis.

One-dimensional nanostructures, such as TiO_2 NWs, enable greater photocatalytic degradation of organic pollutants due to their larger surface area and efficient charge transfer and have attracted keen interest in recent years.[20,27] Binary phase NWs, such as TiO_2-B@anatase NWs, can increase the photodegradation rate of organic compounds by a factor of 5 than the control single-phase photocatalyst as a result of a smaller energy bandgap.[28] In our study, the degradation of MB was chosen as a model reaction to measure the photocatalytic activity of TiO_2-B@anatase NWs. Figure 5D shows the decay of the MB concentration versus UV irradiation time in the aqueous solution with and without TiO_2-B@anatase NWs acting as a photocatalyst. It is obvious that the photocatalyst of TiO_2-B@anatase NWs had greater photocatalytic activity than the sample without NWs. However, the light source and

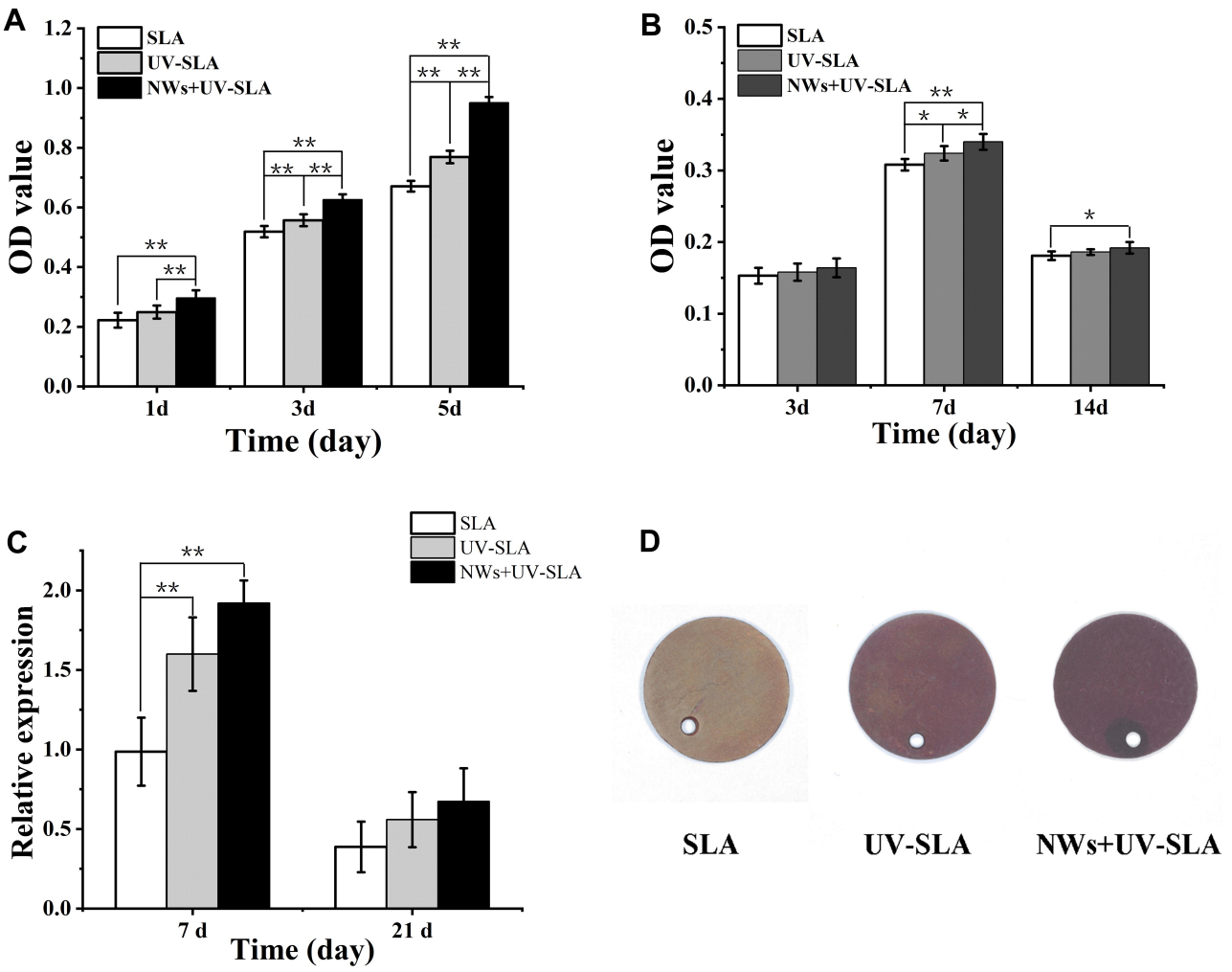

Figure 10 (**A**) Proliferation of cells on titanium surfaces at days 1, 3 and 5. (**B**) The alkaline phosphatase activity of MG-63 cells on different titanium surfaces at days 3, 7 and 14. (mean±SD, n=6; *p<0.05, **p<0.01). (**C**) ALP gene expression in osteoblasts on different titanium surfaces. (mean±SD, n=6; **p<0.01). (**D**) Alizarin red-stained mineralized nodules deposited on different titanium surfaces.

photocatalyst are two indispensable components of photocatalysis. The decrease in the concentration of MB with increasing illumination time can result from the generation of ·OH radicals.[28,30,36] The photooxidation and photoreduction activities of TiO_2 were estimated by detecting the amount of ·OH radicals.[24,37] A few strong oxidants can be generated during photocatalysis, such as O^{2-} and H_2O_2, but they do not interface with the reaction between the ·OH radicals and terephthalic acid.[30] Furthermore, the identical shape and maximum wavelength of the spectrum produced in the present study were consistent with that of 2-hydroxyterephthalic acid (Figure 5A). Similar to the results of a previous study,[30] the larger the amount of the formation of ·OH radicals was, the higher the photocatalytic activity.

In the present work, a new titanium surface cleaning method was developed by performing photocatalysis using TiO_2-B@anatase NWs. Unlike the previous study,[38] photocatalysis of TiO_2-B@anatase NWs effectively removed contamination from the titanium surface without sacrificing the surface topography and roughness. In addition, in most recent studies,[6,7,18,19] titanium surfaces were treated by UV irradiation in air; therefore, the surface is inevitably exposed to air during or after UV irradiation, thereby causing further problems with contamination while complicating further experiments. In our study, the XPS spectra showed that the predominant peak at 284.8 eV, which is ascribed to oxygen-containing hydrocarbons adsorbed onto the SLA surfaces, decreased after UV or NWs+UV treatment but basically remained unchanged after treatment with only NWs (Figure 8A). The 2p3/2 peaks of Ti and TiO_2 were deemed to be at 453.8 eV and 458.5 eV, respectively.[19] In addition, the peaks attributed

to species such as Ti^0, Ti^{2+} and Ti^{3+} were not detected in the lower energy regions among the titanium surfaces of different groups. These results indicated that the very near surfaces of the titanium surfaces were all fully oxidized to stoichiometric TiO_2 thin films. From another point of view, the results also demonstrate that photocatalysis cannot occur without a light source. However, compared to the NWs+UV-SLA group, the photocatalytic activity generated by only the TiO_2 oxide film formed on the UV-SLA surface was substantially lower. Clinical dental implants are typically considered to be contaminated with hydrocarbons, as progressive accumulation of organic molecules is unavoidable in ambient conditions.[12,39] This study demonstrated that contamination, particularly from hydrocarbons, was effectively cleaned under the photocatalysis of the NWs+UV.

The photoinduced superhydrophilicity of TiO_2 thin film was first discovered in 1997.[17] Our results demonstrate that either UV or UV+NWs treatment can generate superhydrophilicity (contact angle <5°) on the SLA surfaces. This unique characteristic is ascribed to the altered molecular structure of the titanium surface generated by photocatalysis of the TiO_2 thin film.[7,18,19] Two mechanisms have been proposed to describe photocatalysis. In this model, strong oxidizing oxygen vacancies generated during hydrocatalysis can result in the conversion of relevant Ti^{4+} sites to Ti^{3+} sites, which is conducive to dissociative water adsorption to form basic Ti-OH. In addition, photocatalysis of TiO_2 can remove contamination on the titanium surface (Figure 11). In fact, for clinical dental implants, there is no information for users to determine when the products were manufactured. However, organic impurities such as hydrocarbons accumulate progressively onto the titanium surface exposed to air.[12,39] In our study, the C 1s peak at approximately 284.8 eV ascribed to hydrocarbons decreased after UV or NWs+UV treatment, while the corresponding atomic percentage of C decreased from 49.49% down to 36.63% and 25.3% after UV or NWs +UV treatment, respectively. Nevertheless, to what extent the generated superhydrophilicity removed hydrocarbons from the titanium is a truly complicated question. Moreover, the hydrocarbons on the NWs+UV-SLA

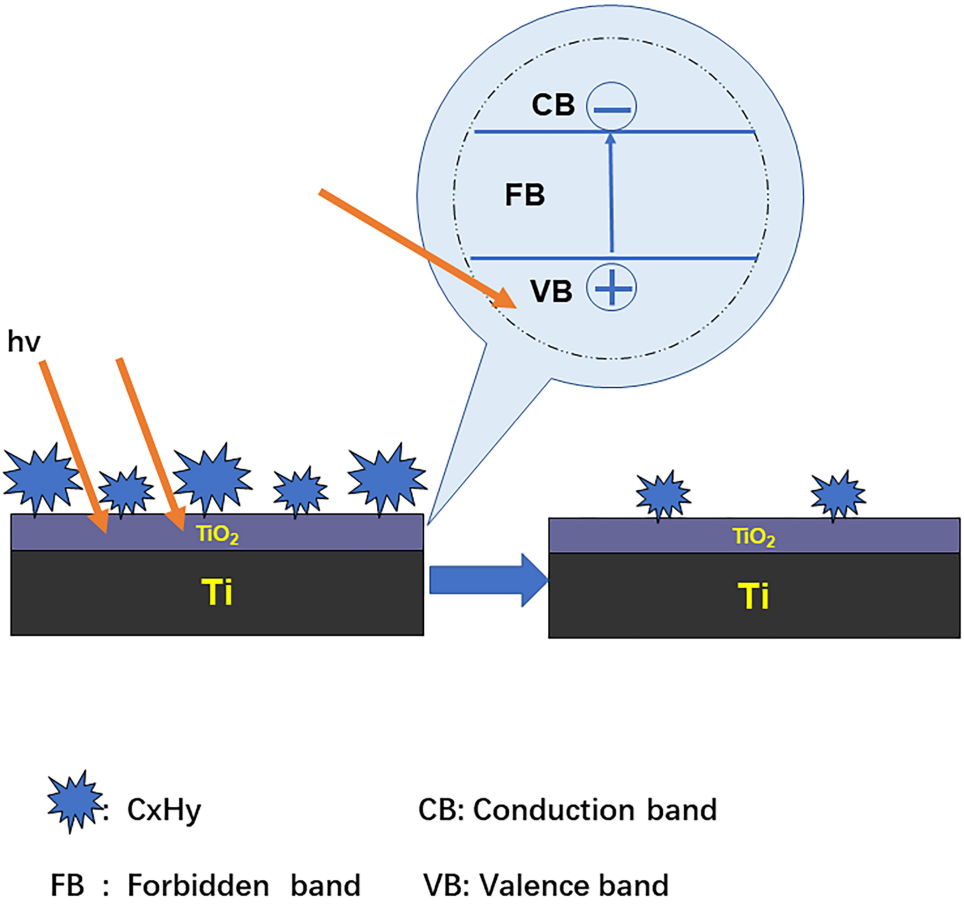

Figure 11 Schematic diagram of the proposed photocatalysis of TiO_2 illustrating the reactivation of the TiO_2 surface that enhances the activity of the titanium surface.

surfaces still could not be completely cleaned, possibly due to insufficient irradiation time or the residual hydrocarbons existing in the oxide film. More importantly, organic impurities inevitably accumulate progressively onto the titanium surface. Meanwhile, the O 1s peak at approximately 531.3 eV fitted to Ti-OH increased after UV or NWs+UV treatment. Ti-OH generation was reported on TiO_2 surfaces during UV light irradiation.[40] Moreover, UV irradiation in water facilitates more basic Ti-OH production than that in air.[32] In this study, the effect of UV or NWs+UV treatment on the amount of Ti-OH formation was similar. As previously mentioned, Ti-OH generation is associated with the dissociative water adsorbed onto the TiO_2 surface. The adsorption of dissociative water on solid surfaces was reported to be sensitive to temperature changes;[41] however, the definitive relationship among them has yet to be clearly reported. Another mechanism of the photoinduced superhydrophilicity of a TiO_2 surface involves desorption of H_2O molecules from the TiO_2 surface by the effect of heating from the absorption of light.[41] Consequently, how the superhydrophilicity of a TiO_2 surface should be modelled is complicated and controversial.

The titanium surfaces cleaned via photocatalysis enhanced the affinity between the biomaterials and the cells. A notable result regarding the initial behaviours of cells was the significantly increased number of migrated and attached cells onto the SLA-UV and NWs+UV-SLA surfaces compared with that of the SLA surfaces. These results revealed that age-related alterations occurred on the SLA surfaces, which diminished their attraction to osteoblast cells. More importantly, the number of migrated and attached cells onto the NWs+UV-SLA surfaces increased even higher than that of the UV-SLA surfaces. The amount of hydrocarbons was strongly correlated with the rates of cell attachment.[19] In light of this theory, the amount of hydrocarbons removed from either the NWs+UV-SLA surfaces or the UV-SLA surfaces was greater than that from the SLA surfaces, which seems to account for the results in our study. However, another study demonstrated that Ti-OH groups enhance cell response.[32] Similarly, both the NWs +UV-SLA surfaces and the UV-SLA surfaces have more Ti-OH groups than do the SLA surfaces. Therefore, the hydrocarbon, Ti-OH groups, or another dominant factor, or the combined effect of them, must be investigated in the future. Furthermore, cell spreading behaviours occurs after the cells attach to biomaterials. Development of a cellular skeleton and extension are necessary steps to initiate cellular functions and intracellular signalling.[18] Apparently, UV and NWs+UV cleaned titanium surfaces facilitated the spread of osteoblasts, which exhibit triangular and polygonal shapes. In particular, some spindle-like filopodias exhibited a more extensive arrangement on the NWs+UV-SLA surfaces. In contrast, the cytoskeletal arrangement on the SLA surfaces was insufficiently spread. In the present results, the NWs +UV-SLA surfaces could be more favourable to cellular attachment and spreading. The interactions between the cells and the biomaterials are complicated and represent a controversial question. Excluding the impact of hydrocarbons and Ti-OH groups on titanium surfaces, the surface electronic charge, surface energy and other properties are required to identify the underlying mechanism.

An inverted correlation between proliferation and differentiation in osteoblasts has been reported.[42] However, in accordance with other studies,[10,18,19,34] the photocatalysis of TiO_2 enhanced osteoblastic proliferation and differentiation. Compared with the other two surfaces, the NWs +UV-SLA surface exhibited greater proliferative activity at 3 d and 5 d of incubation and better ALP activity at 7 d. This behaviour indicated that the titanium surfaces cleaned by photocatalysis are conductive to bone formation around titanium implants, but this must be investigated further. In this phenomenon, a large number of cell signalling pathways and intercellular interactions were increased and were regulated by cellular attachment.[43] Moreover, an aryl hydrocarbon receptor-mediated contamination could influence gene expression and lead to a reduction in the ALP activity of the osteoblasts.[44] Thus, the greater ALP activity may be attributed to the effective removal of hydrocarbons in this study.

The surface chemistry would influence not only the initial bone-implant interaction but also the later bone formation around the implant. Cleanliness, a crucial aspect of surface chemistry, plays an important role in determining the early osseointegration of titanium implants. Organic impurities, such as polycarbonyls and hydrocarbons adsorbed onto titanium surfaces, are considered to be unavoidable under ambient conditions. Thus, the role of surface contamination on the bioactivity of titanium is of great interest and should be the focus of future studies. The photocatalysis of TiO_2 has been widely used in dealing with water pollution. The present study regarding the effect of NWs+UV treatment on the titanium surface indicated that photocatalysis using TiO_2-B@anatase nanowires could effectively remove hydrocarbons. We expect that this technology would be immediately and extensively applied to

cleaning titanium implants, which is an important step in the process of implant production.

Conclusion

In this study, we demonstrated that the photocatalysis of TiO_2-B@anatase NWs could effectively remove hydrocarbons on titanium surfaces without sacrificing the favourable surface morphology. In addition, compared to titanium surfaces without the use of a photocatalytic cleaning process, UV-SLA and NWs+UV-SLA titanium surfaces markedly enhanced cellular migration, attachment, spreading, proliferation and early differentiation, especially on NWs+UV-SLA surfaces. The photocatalytic activity generated by a TiO_2 film that spontaneously formed in air did not sufficiently remove the contamination from the titanium surface. Furthermore, the hydrocarbons on the NWs+UV-SLA surfaces could not be entirely cleaned, which may be attributed to the insufficient irradiation time or the residual hydrocarbons existing in the oxide film. More importantly, organic impurities inevitably accumulate on the titanium surface. Thus, this study provides a new approach for contamination removal from titanium surfaces, which is beneficial for establishing early osseointergration.

Acknowledgments

The study was supported by the Natural Science Foundation of Guangdong Province, China (2018A030310439), the Medical Scientific Research Foundation of Guangdong Province, China (A2019485), the Science Foundation of SMU, China (PY2017N039) and the Foundation of Youthful Innovative talents of General University Guangdong Province (2017KQNCX032).

Disclosure

The authors report no conflicts of interest for this work.

References

1. Albrektsson T, Johansson C. Osteoinduction, osteoconduction and osseointegration. *Eur Spine J*. 2001;2(Suppl 2):S96–S101. doi:10.1007/s005860100282
2. Raghavendra S, Wood MC, Taylor TD. Early wound healing around endosseous implants: a review of the literature. *Int J Oral Maxillofac Implants*. 2005;20(3):425–431.
3. Davies JE. Understanding peri-implant endosseous healing. *J Dent Educ*. 2003;67(8):932–949. doi:10.1002/j.0022-0337.2003.67.8.tb03681.x
4. Micheletti C, Lee BEJ, Deering J, et al. Ti-5Al-5Mo-5V-3Cr bone implants with dual-scale topography: a promising alternative to Ti-6Al-4V. *Nanotechnology*. 2020;31(23):235101. doi:10.1088/1361-6528/ab79ac
5. Dong TS, Duan CY, Wang S, et al. Multifunctional surface with enhanced angiogenesis for improving long-term osteogenic fixation of poly (ether ether ketone) implants. *ACS Appl Mater Interfaces*. 2020;12(13):14971–14982. doi:10.1021/acsami.0c02304
6. Att W, Hori N, Iwasa F, et al. The effect of UV-photofunctionalization on the time-related bioactivity of titanium and chromium-cobalt alloys. *Biomaterials*. 2009;30(26):4268–4276. doi:10.1016/j.biomaterials.2009.04.048
7. Suzuki T, Hori N, Att W, et al. Ultraviolet treatment overcomes time-related degrading bioactivity of titanium. *Tissue Eng Part A*. 2009;15(12):3679–3688. doi:10.1089/ten.TEA.2008.0568
8. Kilpadi DV, Lemons JE, Liu J, et al. Cleaning and heat-treatment effects on unalloyed titanium implant surfaces. *Int J Oral Maxillofac Implants*. 2000;15(2):219–230.
9. Lu H, Zhou L, Wan L, et al. Effects of storage methods on time-related changes of titanium surface properties and cellular response. *Biomed Mater*. 2012;7(5):055002. doi:10.1088/1748-6041/7/5/055002
10. Gao Y, Liu Y, Zhou L, et al. The effects of different wavelength UV photofunctionalization on micro-arc oxidized titanium. *PLoS One*. 2013;8(7):e68086. doi:10.1371/journal.pone.0068086
11. Jofré J, Conrady Y, Carrasco C. Survival of splinted mini-implants after contamination with stainless steel. *Int J Oral Maxillofac Implants*. 2010;25(2):351–356.
12. Massaro C, Rotolo P, Riccardis F, et al. Comparative investigation of the surface properties of commercial titanium dental implants. Part I: chemical composition. *J Mater Sci Mater Med*. 2002;13(6):535–548. doi:10.1023/a:1015170625506
13. Takeuchi M, Martra G, Coluccia S, et al. Investigations of the structure of H_2O clusters adsorbed on TiO_2 surfaces by near-infrared absorption spectroscopy. *J Phys Chem B*. 2005;109(15):7387–7391. doi:10.1021/jp040630d
14. Duddeck DU, Albrektsson T, Wennerberg A, et al. On the cleanliness of different oral implant systems: a pilot study. *J Clin Med*. 2019;8(9):1280. doi:10.3390/jcm8091280
15. Bumgardner JD, Wiser R, Elder SH, et al. Contact angle, protein adsorption and osteoblast precursor cell attachment to chitosan coatings bonded to titanium. *J Biomater Sci Polym Ed*. 2003;14(12):1401–1409. doi:10.1163/156856203322599734
16. Att W, Hori N, Takeuchi M, et al. Time-dependent degradation of titanium osteoconductivity: an implication of biological aging of implant materials. *Biomaterials*. 2009;30(29):5352–5363. doi:10.1016/j.biomaterials.2009.06.040
17. Wang R, Hashimoto K, Fujishima A. Light-induced amphiphilic surface. *Nature*. 1997;388:431–432. doi:10.1038/41233
18. Hori N, Ueno T, Suzuki T, et al. Ultraviolet light treatment for the restoration of aged-related degradation of titanium bioactivity. *Int J Oral Maxillofac Implants*. 2010;25(1):49–62.
19. Aita H, Hori N, Takeuchi M, et al. The effect of ultraviolet functionalization of titanium on integration with bone. *Biomaterials*. 2009;30(6):1015–1025. doi:10.1016/j.biomaterials.2008.11.004.
20. Efstathiou P, Xu X, Menard H, et al. An investigation of crystal structure, surface area and surface chemistry of strontium niobate and their influence on photocatalytic performance. *Dalton Trans*. 2013;42(22):7880–7887. doi:10.1039/c3dt32064b.
21. Tung WS, Daoud WA, Leung SK. Understanding photocatalytic behavior on biomaterials: insights from TiO(2) concentration. *J Colloid Interface Sci*. 2009;339:424–433. doi:10.1016/j.jcis.2009.07.043
22. Watanabe T, Yoshida N. Wettability control of a solid surface by utilizing photocatalysis. *Chem Rec*. 2008;8(5):279–290. doi:10.1002/tcr.20154
23. Tsukimura N, Yamada M, Iwasa F, et al. Synergistic effects of UV photofunctionalization and micro-nano hybrid topography on the biological properties of titanium. *Biomaterials*. 2011;32(19):4358–4368. doi:10.1016/j.biomaterials.2011.03.001

24. Liu G, Sun C, Yang HG, et al. Nanosized anatase TiO_2 single crystals for enhanced photocatalytic activity. *Chem Commun (Camb)*. 2010;46(5):755–757. doi:10.1039/b919895d
25. Movsesyan L, Maijenburg AW, Goethals N, et al. ZnO nanowire networks as photoanode model systems for photoelectrochemical applications. *Nanomaterials (Basel)*. 2018;8(9):693. doi:10.3390/nano8090693
26. Gao Y, Liu Y, Zhao YD, et al. The structure and biological properties of clustered anatase/rutile nanowire array–modified titanium surface. *J Nanopart Res*. 2020;22:76. doi:10.1007/s11051-020-04794-x
27. Walter MG, Warren EL, McKone JR, et al. Solar water splitting cells. *Chem Rev*. 2010;110(11):6446–6473. doi:10.1021/cr1002326
28. Liu B, Khare A, Aydil ES. TiO2-B/anatase core-shell heterojunction nanowires for photocatalysis. *ACS Appl Mater Interface*. 2011;3(11):4444–4450. doi:10.1021/am201123u
29. Yang D, Zhao J, Liu H, et al. Enhancing photoactivity of TiO_2(B)/anatase core-shell nanofibers by selectively doping cerium ions into the TiO_2(B) core. *Chemistry*. 2013;19(16):5113–5119. doi:10.1002/chem.201202719
30. Xiao Q, Ouyang LL. Photocatalytic activity and hydroxyl radical formation of carbon-doped TiO2 nanocrystalline: effect of calcination temperature. *Chem Eng J*. 2009;148(2):248–253. doi:10.1016/j.cej.2008.08.024
31. Liu B, Boercker JE, Aydil ES. Oriented single crystalline titanium dioxide nanowires. *Nanotechnology*. 2008;19(50):505604. doi:10.1088/0957-4484/19/50/505604
32. Han Y, Chen D, Sun J, et al. UV-enhanced bioactivity and cell response of micro-arc oxidized titania coatings. *Acta Biomater*. 2008;4(5):1518–1529. doi:10.1016/j.actbio.2008.03.005
33. Zhao X, Chen J, Zhu Q, et al. Surface characterization of 7S and 11S globulin powders from soy protein examined by X-ray photoelectron spectroscopy and scanning electron microscopy. *Colloids Surf B Biointerfaces*. 2011;86(2):260–266. doi:10.1016/j.colsurfb.2011.03.044
34. Li S, Ni J, Liu X, et al. Surface characteristics and biocompatibility of sandblasted and acid-etched titanium surface modified by ultraviolet irradiation: an in vitro study. *J Biomed Mater Res Appl Biomater*. 2012;100(6):1587–1598. doi:10.1002/jbm.b.32727
35. Linderback P, Harmankaya N, Askendal A, et al. The effect of heat- or ultra violet ozone-treatment of titanium on complement deposition from human blood plasma. *Biomaterials*. 2010;31(18):4795–4801. doi:10.1016/j.biomaterials.2010.02.060
36. Houas A, Lachheb H, Ksibi M, et al. Photocatalytic degradation pathway of methylene blue in water. *Appl Catal B Environ*. 2011;31:145–157. doi:10.1016/s0926-3373(00)00276-9
37. Liu G, Wang LZ, Sun CH, et al. Band-to band visible-light photon excitation and photoactivity induced by homogeneous nitrogen doping in layered titanates. *Chem Mater*. 2009;21(7):1266–1274. doi:10.1021/cm802986r
38. Park JH, Olivares-Navarrete R, Baier RE, et al. Effect of cleaning and sterilization on titanium implant surface properties and cellular response. *Acta Biomater*. 2012;8(5):1966–1975. doi:10.1016/j.actbio.2011.11.026
39. Buser D, Broggini N, Wieland M, et al. Enhanced bone apposition to a chemically modified SLA titanium surface. *J Dent Res*. 2004;83(7):529–533. doi:10.1177/154405910408300704
40. Wang R, Hashimoto K, Fujishima A, et al. Photogeneration of highly amphiphilic TiO_2 surfaces. *Adv Mater*. 1998;10(2):135–138. doi:10.1002/(SICI)1521-4095
41. Takeuchi M, Sakamoto K, Martra G, et al. Mechanism of photoinduced superhydrophilicity on the TiO_2 photocatalyst surface. *J Phys Chem B*. 2005;109(32):15422–15428. doi:10.1021/jp058075i
42. Alborzi A, Mac K, Glackin CA, et al. Endochondral and intramembranous fetal bone development: osteoblastic cell proliferation, and expression of alkaline phosphatase, m-twist, and histone H4. *J Craniofac Genet Dev Biol*. 1996;16(2):94–106.
43. Aita H, Att W, Ueno T, et al. Ultraviolet light-mediated photofunctionalization of titanium to promote human mesenchymal stem cell migration, attachment, proliferation and differentiation. *Acta Biomater*. 2009;5(8):3247–3257. doi:10.1016/j.actbio.2009.04.022
44. Ryan EP, Holz JD, Mulcahey M, et al. Environmental toxicants may modulate osteoblast differentiation by a mechanism involving the aryl hydrocarbon receptor. *J Bone Miner Res*. 2007;22(10):1571–1580. doi:10.1359/jbmr.070615.